JULY 01 2024

Tunable elastic wave transmission and resonance in a periodically aligned tube-block structure

Akira Sasaki; Naoki Mori ; Takahiro Hayashi

J. Acoust. Soc. Am. 156, 44–54 (2024)
https://doi.org/10.1121/10.0026462

JASA ARTICLE

Tunable elastic wave transmission and resonance in a periodically aligned tube-block structure

Akira Sasaki, Naoki Mori,[a] and Takahiro Hayashi
Department of Mechanical Engineering, Graduate School of Engineering, Osaka University, 2-1 Yamadaoka, Suita, Osaka, Japan

ABSTRACT:
A tube-block structure is proposed to realize tunable elastic wave transmission and resonance, consisting of periodically aligned circular tubes sandwiched and joined by two blocks. Finite element simulations for a unit structure are carried out to reveal the frequency dependence of the transmission behavior for the normal incidence of longitudinal and transverse waves in the tube-block structure. As a result, the transmission ratios are found to take multiple local maxima at different peak frequencies. Eigenfrequency analysis shows that the local resonances of the tube and the block surfaces occur at the peak frequencies in the transmission ratios. The peak frequencies originating from the local resonance of the tube depend on its radius and thickness, while those from the resonance on the block surfaces are in good agreement with the theoretical relation between the interval of the periodically aligned tubes and the wavelength of the Rayleigh wave. Furthermore, when the tube-block structure is subjected to compressive loading, the deformation shifts the peak frequencies of the transmission ratio corresponding to the local resonance of the tube. This result implies that the proposed structure has the potential to serve as a tunable meta-interface between solid blocks. © *2024 Acoustical Society of America*. https://doi.org/10.1121/10.0026462

(Received 14 January 2024; revised 3 June 2024; accepted 5 June 2024; published online 1 July 2024)
[Editor: Steffen Marburg] Pages: 44–54

I. INTRODUCTION

Control of elastic wave propagation has gained much attention in recent decades. This technology is not only of academic interest but also plays promising roles in acoustic devices, energy harvesting, etc. Closed-loop resonators, such as ring-type resonators, are one of the widespread components in the design of wave devices. Originally, ring resonators were developed and investigated in optics,[1–4] and their knowledge has been incorporated into acoustics and phononics.[5–8] Robertson *et al.*[8] created a cylindrical waveguide made from polyvinyl chloride (PVC) pipes, showing its application as an add-drop filter for audible acoustic waves. Fu *et al.*[5] fabricated gallium nitride (GaN) strips on sapphire substrates as a ring-shaped waveguide, which can confine and control phonons. In general, to efficiently induce wave interference, the operating wave mode is designed to be single, and the propagation path in a closed-loop waveguide is set sufficiently longer than the wavelength at the operating frequency.

Acoustic metamaterials enable wave control, direction, and manipulation with subwavelength structures, which cannot be observed in natural materials. Numerous studies were reported in the area of the acoustic metamaterials. For example, phononic crystals have periodic or partially periodic structures, which lead to multiple scattering and local resonance. This brings unique features, such as stopbands and waveguiding of acoustic waves.[6,9–13] Kaya *et al.*[6] incorporated a one-dimensional phononic crystal into a ring-type resonator and applied it to gas sensing. Another approach in the design of acoustic metamaterials is to create local resonant structures at subwavelength scales, which are not necessarily periodic.[14–19] Basically, many acoustic metamaterials show inherent characteristics in accordance with input waves.

Nowadays, tunable acoustic metamaterials are extensively investigated to realize variable features in response to input waves. In previous studies, various tuning mechanisms and accompanying metamaterials were proposed, including the use of mechanical,[20–27] piezoelectric,[28–31] and heat[32–34] phenomena. In particular, when some metamaterials undergo deformation, different wave propagation characteristics can appear due to the change in the shapes of the local structures. Babaee *et al.*[22] designed an array of elastomeric helices stretched by two plates, which can be used for an acoustic switch controlled by the deformation. Zhou *et al.*[24] proposed an elastic membrane with bonded metal particles for a membrane-type soft acoustic metamaterial. They showed numerically that its band structure depends on the applied deformation. These ideas seem applicable to acoustic closed-loop resonators. However, to the authors' knowledge, this possibility has not been explored yet.

The present study aims to realize tunable transmission and resonance of elastic waves incorporating the concept of closed-loop resonators and local resonances. To this purpose, a periodically aligned tube structure sandwiched and joined by solid blocks, called a tube-block structure,[35] is proposed in the present paper. The transmission characteristics of the elastic waves across the tube-block structure are analyzed by finite element (FE) simulations. Eigenfrequency

[a]Email: n.mori@mech.eng.osaka-u.ac.jp

https://doi.org/10.1121/10.0026462

analysis is also performed to relate the wave transmission behavior to the local resonances in the structure. Subsequently, mechanical loading is considered in the proposed model to show the tunability of the resonance characteristics. If the tunability is confirmed, the proposed structure would have some possible applications. For example, if some of the resonance frequencies of the proposed structure are affected by compressive loading, it has the potential to be a sensing device that quantifies applied loads by measuring the changes in the resonance frequencies. Furthermore, the variable resonance characteristics could be utilized for a tunable elastic wave filter.

This paper is structured as follows. In Sec. II, the periodic tube-block structure is proposed and described in detail. In Sec. III, the numerical model and method for the elastic wave propagation analysis are explained. The numerical results are presented in Sec. IV. The mechanism of the wave resonance is examined based on the eigenfrequency analysis. Finally, it is shown that some resonance peaks can be shifted by preloads applied to the structure.

II. DESCRIPTION OF STRUCTURE

As shown in Fig. 1(a), a structure consisting of semi-infinite blocks and infinite circular tubes is considered in the Cartesian xyz coordinates. The tubes are periodically aligned in the x direction, sandwiched by the two blocks. The normal lines of the block surfaces are set parallel to the y axis, and the z axis corresponds to the axial direction of the tubes. Figure 1(b) shows the two-dimensional (2D) model under the plane strain condition in the xy plane. The outer radius and thickness of the circular tubes are denoted by R and h, respectively, and their interval is given as W. The whole structure is modeled as a homogeneous, isotropic, and linear elastic material of mass density ρ, longitudinal wave velocity c_L, and transverse wave velocity c_T. The tubes and blocks are joined with a width of $2a$, where the displacement and stress components are assumed to be continuous. The normal approach of the tubes is calculated as $\delta_N = R - \sqrt{R^2 - a^2}$, which is minute compared to the tube radius R. The distance between the surfaces of the two blocks is expressed as $H_{TB} = 2(R - \delta_N)$. Namely, when the upper surface of the bottom block is set as $y = 0$, the lower surface of the top block is located at $y = H_{TB}$. When a plane elastic wave propagating in the y direction is incident on the tubes, analogous behavior to layer resonance[36,37] is expected to occur.

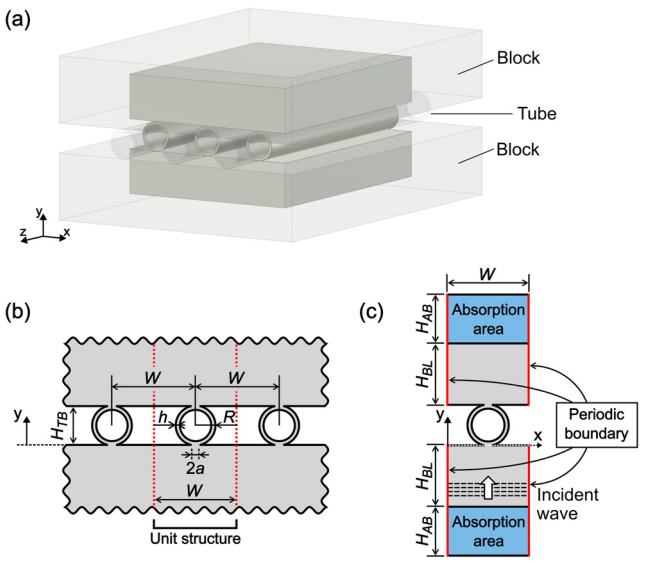

FIG. 1. (Color online) Schematics of (a) the periodic structure consisting of solid blocks and tubes, (b) the 2D structure under the plane-strain condition, (c) its unit structure for the numerical simulation. Circular tubes are aligned periodically with an interval of W in the x direction and sandwiched between two solid blocks.

If the wavefront of the incident wave has an infinite width in the x direction, the numerical model can be simplified by a periodic boundary condition. Figure 1(c) shows a unit structure containing a single tube between the two blocks. The displacement and traction components are set to be equal at the left and right edges of the blocks, denoted as $x = 0$ and W, respectively. The other surfaces of the blocks and the tube are set to be traction-free. In Sec. III, the numerical model and method for the proposed structure are described in detail.

III. NUMERICAL MODEL AND METHOD

The wave propagation behavior in the periodic tube-block structure obeys the 2D Navier's equation in the frequency domain,[38] i.e.,

$$\left(c_L^2 - c_T^2\right)\frac{\partial}{\partial x}\left(\frac{\partial u_x}{\partial x} + \frac{\partial u_y}{\partial y}\right) + c_T^2\left(\frac{\partial^2}{\partial x^2} + \frac{\partial^2}{\partial y^2}\right)u_x = -\omega^2 u_x,$$
$$\left(c_L^2 - c_T^2\right)\frac{\partial}{\partial y}\left(\frac{\partial u_x}{\partial x} + \frac{\partial u_y}{\partial y}\right) + c_T^2\left(\frac{\partial^2}{\partial x^2} + \frac{\partial^2}{\partial y^2}\right)u_y = -\omega^2 u_y, \quad (1)$$

where $\omega = 2\pi f$ is angular frequency, and u_x and u_y are the displacement components in the x and y directions, respectively. It is noted that the displacement components are expressed in the frequency domain. The time-dependent terms are represented as $\exp(i\omega t)$, where $i = \sqrt{-1}$ and t is time.

The finite element method (FEM) was employed to examine the elastic wave propagation in the structure of Fig. 1(c). The whole structure was approximated as the assembly of finite elements. To model the semi-infinite blocks in the y direction, absorbing regions were arranged on the outer sides of the elastic blocks with a height of H_{BL}, i.e., $y < -H_{BL}$ and $y > H_{TB} + H_{BL}$. The height of the absorbing regions is denoted by H_{AB}. The absorbing regions have material properties with non-zero imaginary parts and exhibit a wave-damping effect that gradually increases toward the upper and lower edges, as proposed in Ref. 39. These regions can eliminate the edge reflections in the y direction. Either purely longitudinal (L) or transverse (T) plane wave is incident on the tube-block structure, excited by applying the stress components at $y = -H_{BL}$. In the case

of the L wave incidence, the normal stress component σ_y is prescribed uniformly at $y = -H_{BL}$, while the shear stress component τ_{xy} is uniformly applied to excite the T wave.

The transmission behavior of the elastic waves across the tube is quantified by the time-averaged energy flux in the y direction a,

$$E_{Tr} = \frac{\omega}{2}\int_0^W \mathrm{Im}\left(\tau_{xy}^* u_x + \sigma_y^* u_y\right)\mathrm{d}x, \tag{2}$$

calculated along the cross section at $y = H_{TB} + H_{BL}$, where the superscript * represents the complex conjugate. The transmission ratio is defined as

$$T = \frac{E_{Tr}}{E_0}, \tag{3}$$

where E_0 is the time-averaged energy flux for a single block of height $H_{TB} + 2H_{BL}$ sandwiched by absorbing regions. The time-averaged energy flux E_0 is calculated by Eq. (2), similarly to E_{Tr}. The numerical simulation described above was carried out in the frequency range of $f = 10$–100 kHz with a frequency increment of 0.2 kHz.

A commercial FE analysis software COMSOL Multiphysics (COMSOL Inc., Stockholm, Sweden) was used to numerically solve Eq. (1). The tube-block structure was assumed to be made from aluminum alloy with the wave velocities $c_L = 6.40$ km/s and $c_T = 3.17$ km/s and the mass density $\rho = 2.70 \times 10^3$ kg/m^3. Second-order Lagrange elements were employed in the discretization of the structure. Basically, the element size should be set sufficiently small compared to the minimum wavelength in the frequency range of interest, i.e., the wavelength of the T wave $\lambda_T = 31.7$ mm at $f = 100$ kHz. However, this setting can be insufficient for joints between the tube and the blocks, which are characterized as the joint width $2a$. Accordingly, the element size at the joints was set as $0.3a$ to guarantee the calculation accuracy, while the remaining part was discretized by elements whose size was smaller than $0.1\lambda_T$.

IV. RESULTS AND DISCUSSIONS

A. Frequency dependence of transmission ratios

Wave propagation analysis was performed for the tube-block structure with dimensions of $W = W_0 = 40$ mm, $R = R_0 = 10$ mm, $h = h_0 = 2.0$ mm, and $2a = 2a_0 = 0.1$ mm. The transmission ratio T was calculated for each incident frequency by Eq. (3). Figure 2 shows the frequency dependence of the transmission ratios for the incidence of the L and T waves. Both transmission ratios take six peaks, but their peak behavior is found to be different. The peaks in the transmission ratios of the L and T waves are labeled as L1–L6 and T1–T6, respectively. For the L wave incidence, the peaks of L1–L6 look separated from each other. On the other hand, for the T wave incidence, the three peaks of T2–T4 are overlapped, while the other peaks appear individually. It is expected that the dimensions of the structure and the incident wave mode affect the peak locations.

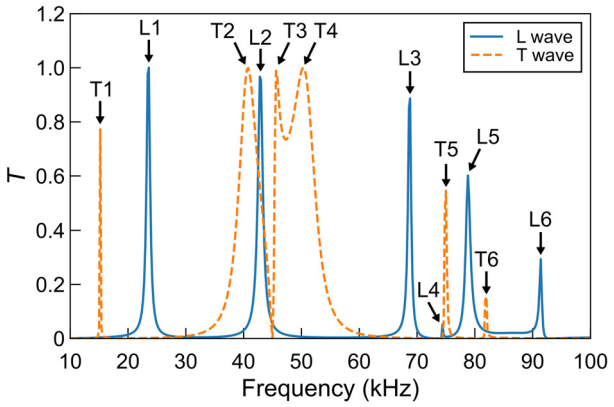

FIG. 2. (Color online) Variation of the transmission ratios with frequency for the incidence of L and T waves, calculated at fixed dimensions $W = W_0$, $R = R_0$, $h = h_0$, and $2a = 2a_0$.

The effects of the tube radius R and the tube thickness h on the transmission ratio are first examined for the L wave incidence. The tube interval W and the joint width $2a$ are fixed at $W = W_0$ and $2a = 2a_0$, respectively. Figures 3(a) and 3(b) show the transmission ratios obtained for different tube radii R and tube thicknesses h, respectively. The tube thickness is fixed at $h = h_0$ in Fig. 3(a), while the tube radius is $R = R_0$ in Fig. 3(b). For the L wave incidence, it is shown in Fig. 3(a) that as the tube radius R increases, the frequencies of the peaks except for L4 tend to decrease. These peaks shift rightward as the tube thickness h increases, as shown in Fig. 3(b). On the other hand, the changes in the tube radius R and the tube thickness h do not give rise to a clear shift of the peak L4.

Different trends appear in the transmission ratio for the T wave incidence. Figures 3(c) and 3(d) show the transmission ratios of the T wave for different tube radii R and tube thicknesses h, respectively. In Fig. 3(c), the peak frequencies of T1–T4 and T6 decrease with increasing tube radius R, but the peak T5 looks unshifted. This behavior is analogous to the variation of the L wave transmission ratio shown in Fig. 3(a). However, the effects of the tube thickness h on the peak frequencies are more complex. In Fig. 3(d), the increase in the tube thickness h leads to the increase in the peak frequencies of T1, T3, and T6 but to the decrease in the peak frequencies of T4. The variation of the peak frequency T2 appears to be nonmonotonic. Regarding the peak T5, its frequency is 75.2 kHz at $h = 1.8$ mm and 75.0 kHz at $h = 2.0$ mm and 2.2 mm, which implies that the location of the peak T5 is nominally invariant with the tube thickness h and show similar dependence on the tube radius R. These features are further examined in Sec. IV B, based on the vibration characteristics of the structure at each peak frequency.

The transmission ratios were calculated for different tube intervals W. Figures 4(a) and 4(b) show the frequency dependence of the transmission ratios for the L and T wave incidence, respectively. The other dimensions were fixed at $R = R_0$, $h = h_0$, and $2a = 2a_0$. For the L wave incidence, as shown in Fig. 4(a), the peak frequencies of L3–L5 decrease

https://doi.org/10.1121/10.0026462

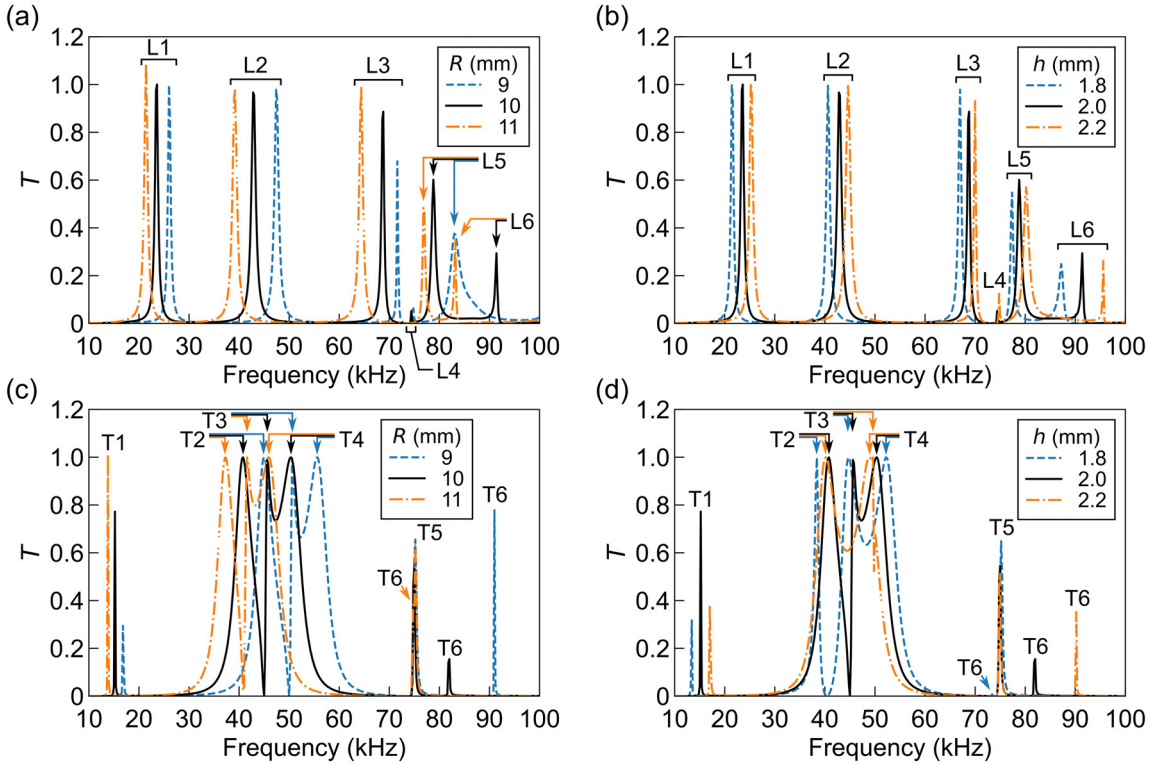

FIG. 3. (Color online) Variation of the transmission ratios with frequency for the L wave incidence, calculated for different (a) tube radii R at $h = h_0$ and (b) tube thicknesses h at $R = R_0$. (c) and (d) show the transmission ratios for the T wave incidence, obtained for different tube radii R and tube thicknesses h, respectively. The tube interval W and the joint width $2a$ are fixed at $W = W_0$ and $2a = 2a_0$, respectively.

as the tube interval W increases, while the shifts of the other peaks are trivial. A similar tendency can be observed for the T wave incidence in Fig. 4(b). Namely, only the peak T5 shifts leftward as the tube interval W increases.

The effects of the joint width $2a$ on the transmission ratios are examined for the incidence of the L and T waves in Figs. 5(a) and 5(b), respectively. The variation of the joint width in $0.05\,\text{mm} < 2a < 0.15\,\text{mm}$ affects some of the peak locations. The peak frequencies of L2, L3, and L5 in Fig. 5(a) and T2 and T4 in Fig. 5(b) tend to increase as the joint width $2a$ increases. It is noted that the joint width is far shorter than the minimum wavelength in the frequency range of interest, i.e., $\lambda_T = 31.7\,\text{mm}$ at $f = 100$ kHz. The dependence of the peak frequencies on different structure dimensions is discussed in Secs. IV B and IV C. Hereafter, the joint width is fixed at $2a = 0.1\,\text{mm}$ for simplicity.

B. Mechanism of peak appearance

It has been shown in Sec. IV A that the transmission ratios for the tube-block structure have peaks at multiple frequencies. Some peak frequencies depend on the tube radius R and the tube thickness h, but the others remain unshifted. In this section, the wavefield at each peak frequency is investigated to clarify the peak behavior of the transmission ratios.

For the L wave incidence, the distributions of the displacement magnitude in the vicinity of the tube at the peak frequencies of L1–L4 are shown in Figs. 6(a)–6(d), respectively. In Figs. 6(a) and 6(b), i.e., at the peak frequencies of L1 and L2, the vibrations appear localized at the tube. This feature was also seen at the peak frequency of L6. On the other hand, at the peak frequency of L4, the vibration localized on the surfaces of the blocks is relatively dominant, as shown in Fig. 6(d). The wavefield at the peak frequency of L3 in Fig. 6(c) is similar to Figs. 6(a) and 6(b), but the vibration is also confirmed on the block surfaces. These results correspond to different dependence of the peak frequencies on the structure dimensions. It has been shown in Figs. 3(a) and 3(b) that the peak frequencies of L1 and L2 are affected by the dimensions of the tube, i.e., R and h, while the peak frequency of L4 is nominally invariant with R and h. Since the vibrations at the peak frequency of L3 can be seen at the tube and on the block surfaces, its peak location in the transmission ratio depends on the tube interval W, as well as the tube dimensions R and h.

The displacement distributions at the peak frequencies are also examined for the T wave incidence. Figures 6(e)–6(g) show the wavefields at the peak frequencies of T1–T3, respectively. The displacement fields show localized distributions at the tube, which have the same tendency as the case for the L wave incidence, i.e., Figs. 6(a) and 6(b). This behavior was also observed at the peak frequencies of T4 and T6. These peak frequencies depend on the tube radius R and the tube thickness h, as shown in Figs. 3(c) and 3(d). At the peak frequency of T5, the displacement distribution is localized on the surface of the upper block, as shown in Fig. 6(h). It is noted that the peak frequency of T5 is not

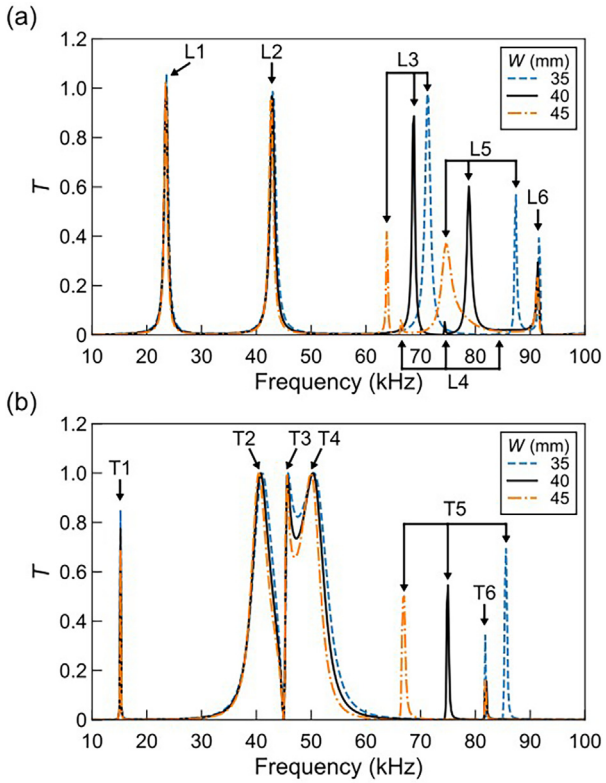

FIG. 4. (Color online) Variation of the transmission ratios with frequency for the (a) L wave and (b) T wave incidence, calculated for different tube intervals W at fixed tube dimensions $R = R_0$, $h = h_0$ and $2a = 2a_0$.

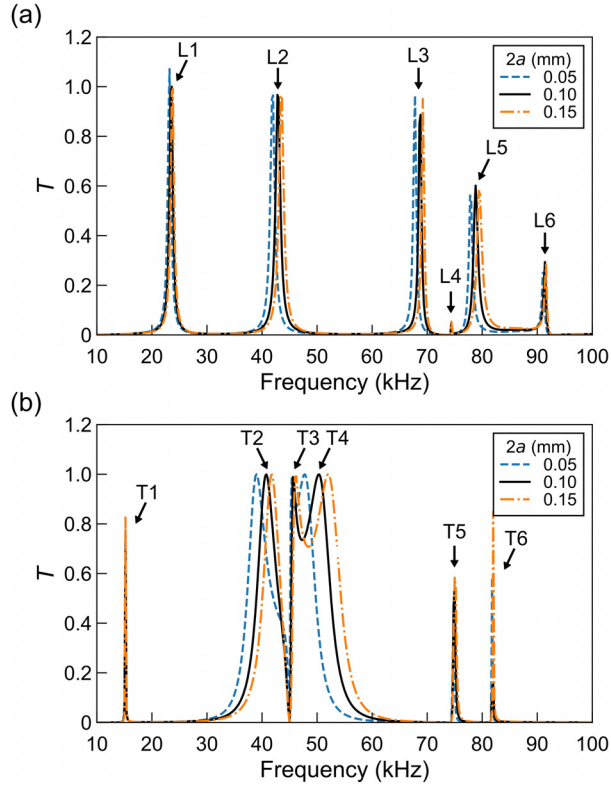

FIG. 5. (Color online) Effects of the joint width $2a$ on the frequency dependence of the transmission ratios for the incidence of the (a) L and (b) T waves. The other dimensions are fixed at $W = W_0$, $R = R_0$, $h = h_0$.

affected by the tube radius R and the tube thickness h, which has been shown in Figs. 3(c) and 3(d). In Sec. IV A, the peak frequencies of the transmission ratios show different dependence on the tube radius R and the tube thickness h. This feature is discussed in Sec. IV C.

The displacement distributions at the peak frequencies of L4 and T5, shown in Figs. 6(d) and 6(h), respectively, imply that these peaks are closely associated with the Rayleigh waves propagating along the block surfaces. At fixed tube dimensions, i.e., $R = R_0$ and $h = h_0$, numerical simulations were performed for different tube intervals W, and the peak frequencies of L4 and T5 were extracted from the transmission ratios. Figure 7 shows the variation of the two peak frequencies with the tube interval W. The obtained peak frequencies decrease monotonically with increasing the tube interval W.

If the Rayleigh wave resonance results in the peak behavior of the transmission ratios, its wavelength λ_R is expressed as $\lambda_R = W$ due to the periodicity of the tube alignment. Namely, the corresponding peak frequency f_R is theoretically predicted as

$$f_R = \frac{c_R}{W}, \tag{4}$$

where c_R is the velocity of the Rayleigh wave, which is well approximated by[38]

$$c_R = m(\kappa)c_T \cong \frac{0.87 + 1.12\nu}{1 + \nu}c_T, \tag{5}$$

where $\nu = (\kappa^2 - 2)/2(\kappa^2 - 1)$ is Poisson's ratio, and $m(\kappa)$ is the function of the wave velocity ratio $\kappa = c_L/c_T$. The theoretical relation of Eq. (4) is plotted together in Fig. 7, showing good agreement with the peak frequencies obtained by the FE simulation. The above discussion indicates that the peaks L4 and T5 in the transmission ratios appear due to the Rayleigh wave resonance, which results from the periodic arrangement of the tubes. This consequence is consistent with the fact that the effect of the tube dimensions on the peak frequencies of L4 and T5 is insignificant.

When the wavefields are localized in the tube, the vibration characteristics of the tube affect the peaks of the transmission ratios. To further examine the mechanism of the peak appearance, eigenfrequency analysis was performed in the frequency range of 10–100 kHz for the tube-block structure at dimensions of $W = W_0$, $R = R_0$, and $h = h_0$. Figure 8 shows the eigenfrequencies corresponding to the peaks in the transmission ratios, plotted with the data shown in Fig. 2. As a result, relative errors between the eigenfrequencies and the peak frequencies obtained by the wave propagation analysis were lower than 1.14%, which shows that the resonance of the structure leads to the peak behavior of the transmission ratios.

The mode distributions at the eight eigenfrequencies are shown in Figs. 9(a)–9(h), corresponding to the peak frequencies obtained by the wave propagation analysis in Figs. 6(a)–6(h), respectively. In Figs. 9(a), 9(b), and 9(e)–9(g), the vibrations are localized at the tube and are similar to the

https://doi.org/10.1121/10.0026462

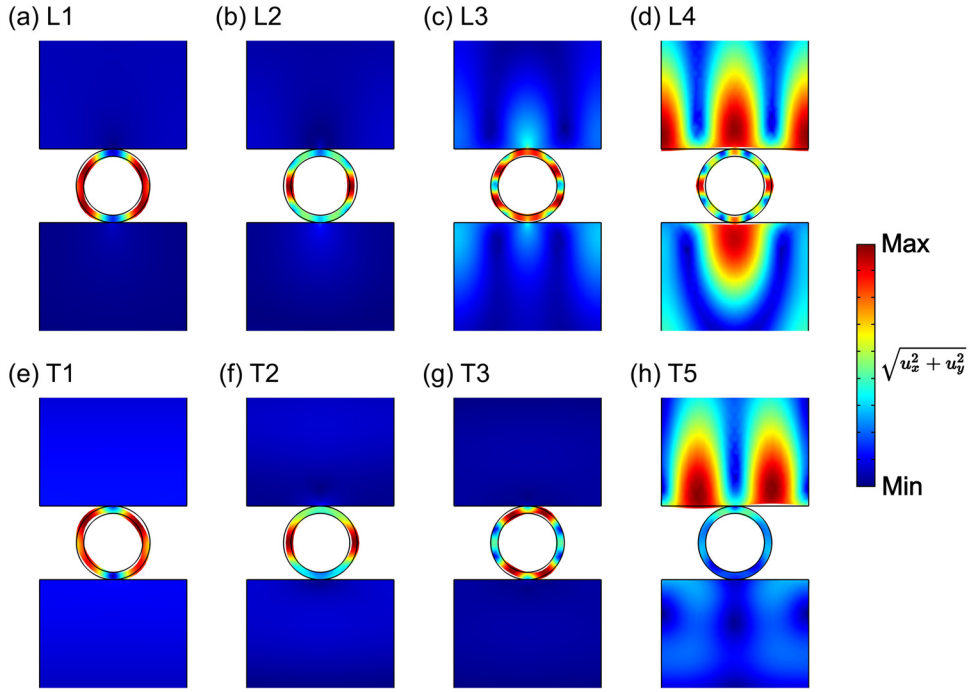

FIG. 6. (Color online) Displacement distributions at the peak frequencies of (a) L1, (b) L2, (c) L3, (d) L4 for the L wave incidence, (e) T1, (f) T2, (g) T3, and (h) T5 for the T wave incidence. The dimensions of the structure are set as $W = W_0$, $R = R_0$, $h = h_0$. The color represents the magnitude of the displacement vector.

displacement distributions in Figs. 6(a), 6(b), and 6(e)–6(g), respectively. This agreement shows that the transmitted wave across the tube is amplified when the incident wave induces the local resonance of the tube. If the vibration of the tube overwhelms that of the blocks, the resonance behavior depends mainly on the vibration characteristics of a single tube, not on the tube interval W. This feature seems true of the peak frequencies L1, L2, and T1–T3. On the other hand, the vibration of the block surfaces is non-negligible in Fig. 9(c), which corresponds to the peak frequency of L3. For this reason, the location of the peak L3 would be affected not only by the tube dimensions R and h but also by the tube interval W. It is noted that the eigenfrequencies corresponding to the peaks L4 and T5, which are related to the Rayleigh wave resonance, can also be obtained by this analysis, as shown in Figs. 9(d) and 9(h).

The mode distributions can also be used to discuss the effects of the joint width $2a$ on the peak frequencies shown in Figs. 5(a) and 5(b). For example, the location of the peak L1 looks unshifted if the joint width $2a$ varies. The vibration pattern of the tube at the peak frequency of L1, i.e., Fig. 9(a), shows that the joints between the tube and the blocks correspond to nodes. This feature would lead to the insensitivity of the peak frequency L1 to the joint width $2a$. In the case of the peak frequency L4, the locations of the joints correspond to anti-nodes in Fig. 9(d). Nevertheless, the effect of the joint width $2a$ on the peak frequency L4 is insignificant probably because this phenomenon is

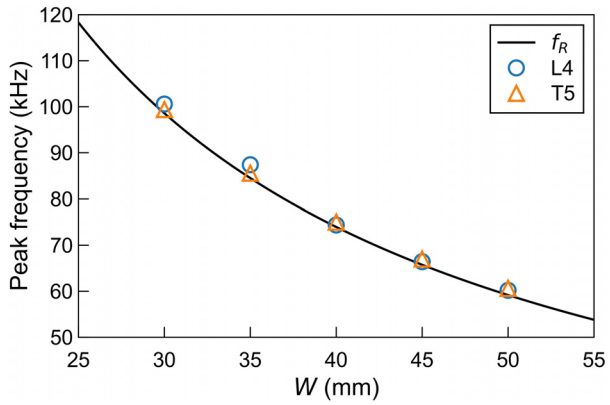

FIG. 7. (Color online) Variation of the peak frequencies of L4 and T5 with the tube interval W, together with the theoretical prediction based on the Rayleigh wave resonance on the block surfaces.

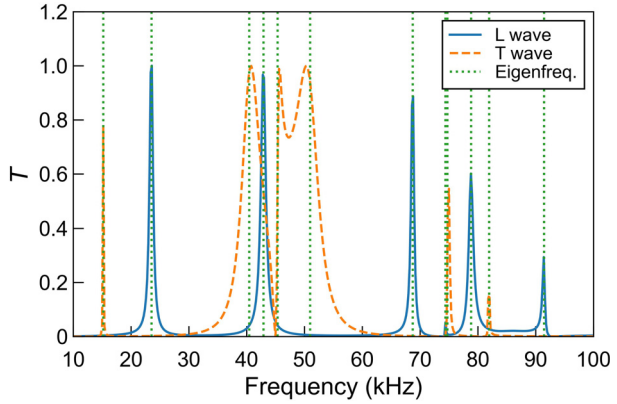

FIG. 8. (Color online) Comparison of the peak frequencies in the transmission ratios for the L and T wave incidence to the eigenfrequencies corresponding to the vibration modes.

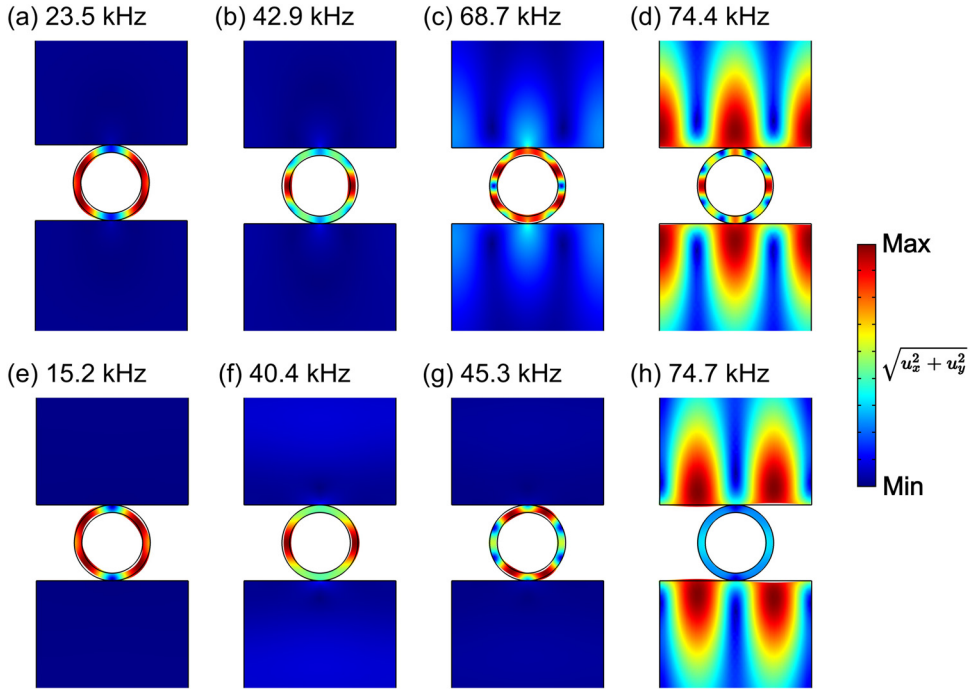

FIG. 9. (Color online) Mode distributions at (a) 23.5, (b) 42.9, (c) 68.7, and (d) 74.4 kHz corresponding to the peaks L1–L4, respectively, and (e) 15.2, (f) 40.4, (g) 45.3, and (h) 74.7 kHz for the peaks T1–T3 and T5, respectively, obtained by eigenfrequency analysis for the structure at $W = W_0$, $R = R_0$, and $h = h_0$. The color represents the magnitude of the displacement vector in each figure.

dominated by the Rayleigh wave resonance. Namely, the tube interval W serves as a source of the Rayleigh wave, which is not significantly affected by the joint width $2a$. Similar discussions can be made for the other peak frequencies in the transmission ratios.

The above numerical analyses have shown that the transmission ratios for the normal wave incidence take peaks at frequencies related to the local resonance of the tube and the Rayleigh wave resonance in the proposed structure. Similar behavior is expected in the oblique wave incidence on the tube array, but the effect of the incident angle on the wave resonance is not explored in the present study.

C. Normalization for rearrangement of FE results

As shown in Sec. IV B, the peaks of the transmission ratios for the tube-block structure result from the two different phenomena, i.e., the Rayleigh wave resonance in the tube alignment direction and the local resonance of the tube. Thus, the theoretical knowledge about the two phenomena is expected to be applicable to rearrange and summarize the numerical results of the peak frequencies in the normalized form. This representation would be useful when designing the dimensions of the structure for given resonance frequencies.

Regarding the peaks originating from the Rayleigh wave resonance, their peak frequencies are well approximated by Eq. (4). This equation can be rewritten in a non-dimensional form as

$$\xi_{\mathrm{R}} = \frac{2\pi}{\gamma} m(\kappa), \tag{6}$$

where $\xi_{\mathrm{R}} = 2\pi f_{\mathrm{R}} R/c_{\mathrm{T}}$ is the normalized peak frequency, and $\gamma = W/R$ is the normalized tube interval. The radius of the tube R is used as a representative length in the normalization.

A similar treatment is applied to the peak frequencies derived from the local resonance of the tube. Gazis[40] analyzed the free vibration of a cylindrical tube with the inner and outer surfaces traction-free, expressing the characteristic equation by using four non-dimensional quantities as

$$F(n, \delta, \kappa, \xi_{\mathrm{TB}}) = 0, \tag{7}$$

where n is the mode order, $\delta = h/R$ is the thickness-radius ratio, $\xi_{\mathrm{TB}} = 2\pi f_{\mathrm{TB}} R/c_{\mathrm{T}}$ is the normalized eigenfrequency, and f_{TB} is the eigenfrequency of the tube. This formula corresponds to the circumferential resonance of the guided wave modes in cylindrical pipes.[41] The boundary condition of the tube in the present study, i.e., cylindrical tubes sandwiched by the solid blocks, is not identical to Gazis's model,[40] but the theoretical background seems similar.

Based on the above formulations, the numerical results of the transmission ratios are rearranged. The wave velocity ratio is fixed at $\kappa = 2.02$, which corresponds to the material property of aluminum alloy. Figure 10(a) shows the transmission ratios for the L wave incidence as functions of the normalized frequency $\xi = 2\pi f R/c_{\mathrm{T}}$, which were calculated for different tube radii R at fixed thickness-radius ratio $\delta = h/R = 0.2$ and normalized tube interval $\gamma = W/R = 4.0$. It is found in this figure that the peaks in the transmission ratio are overlapped even if the value of R changes. The transmission ratio for the T wave incidence shows a similar trend in

https://doi.org/10.1121/10.0026462

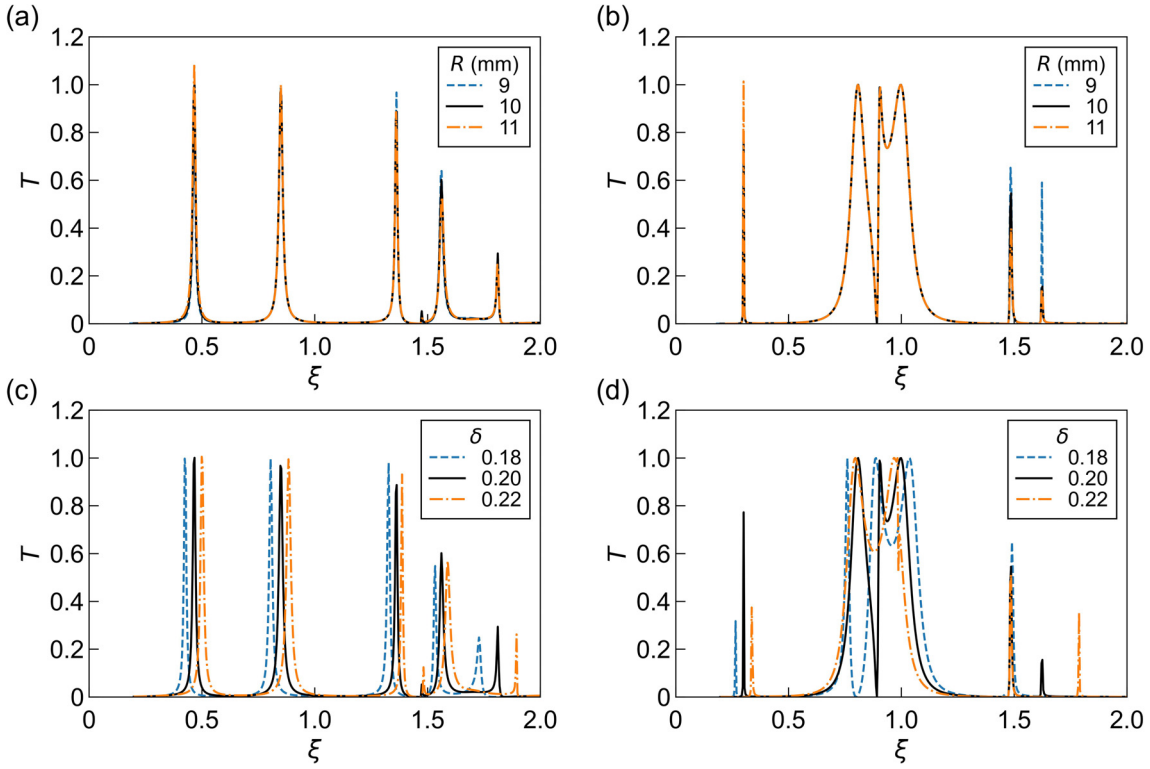

FIG. 10. (Color online) Variation of the transmission ratios for the incidence of the (a) L wave and (b) T wave with the normalized frequency, calculated for different tube radii R at fixed thickness-radius ratio $\delta = 0.2$ and normalized tube interval $\gamma = W/R = 4.0$. (c) and (d) show the transmission ratios for the incidence of the L and T waves, respectively, obtained for different thickness-radius ratios δ at a fixed tube interval $\gamma = 4.0$.

Fig. 10(b). Namely, at fixed thickness-radius ratio δ and normalized tube interval γ, the normalized peak frequencies ξ_{TB} are unchanged if the tube radius R is changed. This result seems consistent with the above theoretical consideration that the normalized resonance frequencies of the tube ξ_{TB} are determined by n, δ, and κ, as suggested in Eq. (7). If the boundary conditions are modified in the theoretical modal analysis following the tube-block structure, the characteristic equation for the local resonance frequencies of the tube could be derived instead of Eq. (7). However, this consideration is not further pursued in the present study.

The numerical analysis is carried out for different thickness-radius ratios δ at a fixed tube interval $\gamma = 4.0$. Figures 10(c) and 10(d) show the transmission ratios as functions of the normalized frequency ξ for the L and T wave incidence, respectively. In both figures, the normalized peak frequencies corresponding to the local resonance of the tube increase with increasing δ. It has been mentioned in Secs. IV A and IV B that the peak frequencies of the transmission ratios vary with the tube radius R and the tube thickness h in different manners. In the case of a single tube, Ref. 40 theoretically shows the effects on the natural frequencies, which bring monotonic or nonmonotonic variation depending on the vibration modes. For the tube-block structure, the variation of the peak frequencies can be similarly rearranged by the normalized quantities. The results obtained in this section show that the normalization procedure is useful for expressing the characteristics of the elastic wave resonance in the tube-block structure.

D. Shift of peak frequency by tube deformation

Section IV B presented that some peaks in the transmission ratio for the L wave incidence result from the local resonance of the tube. This implies that the peak locations can move if the vibration characteristics of the tube are varied somehow, e.g., by its deformation. In order to consider this possibility, the tube-block structure subjected to vertical compressive loading is considered in the present section, as shown in Fig. 11. The geometries of the structure are the same as that in Fig. 1, but a distributed load p is applied uniformly on the end of the upper absorbing region $y = H_{TB} + H_{BL} + H_{AB}$. The displacement components on the end of the lower absorbing region are constrained to zero to avoid rigid translation. It is mentioned here again that the structure is linear elastic. In other words, its response to the compressive loading is assumed to be within linear elastic deformation.

Acoustoelastic analysis[42,43] was carried out to investigate the effects of the static loading on the transmission characteristics of the elastic waves across the tube-block structure. First, the static deformation was analyzed to obtain the displacement and stress fields induced by the compressive load. Then, elastic wave propagation behavior was examined for the prestressed structure in a similar manner to Sec. III. For the incidence of a plane L wave, the transmission ratio across the tube was calculated in the frequency domain.

The above analyses were performed for several different compressive loads. Figures 12(a) and 12(b) show the

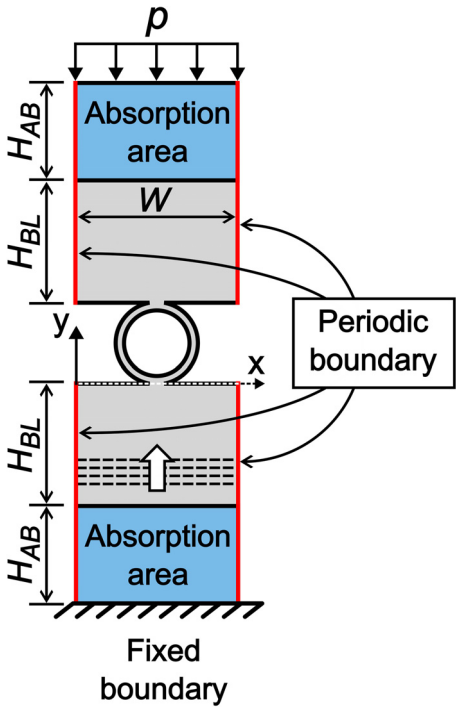

FIG. 11. (Color online) Schematic of the tube-block structure subjected to compressive loading. Displacement components at the lower end of the absorbing region are fixed as zero.

static deformation induced by the compressive load $p = 0.75$ MPa at two tube thicknesses of $h = 1.0$ mm and 2.0 mm, respectively. It is noted that the deformations in these figures are enlarged by five times. The tube radius, tube interval, and joint width were fixed at $R = 10$ mm, $W = 40$ mm, and $2a = 0.1$ mm, respectively. The deformation of the tube at $h = 1.0$ mm in Fig. 12(a) is larger than the one at $h = 2.0$ mm in Fig. 12(b). The maximum Mieses stress in the tube-block structures except for the joint parts was approximately 300 MPa, which is comparable to the 0.2% offset yield stress of aluminum alloy.

Based on the results of the static deformation, the transmission ratios were calculated for the L wave incidence. Figures 13(a) and 13(b) show the frequency dependence of the transmission ratios obtained for $h = 1.0$ mm

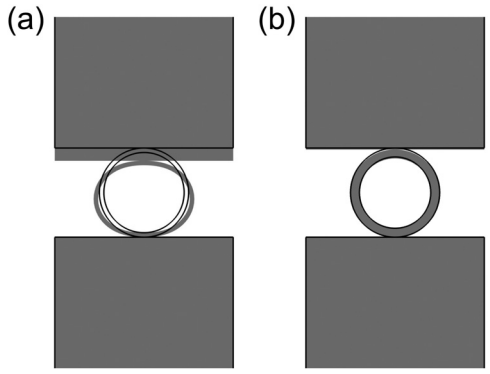

FIG. 12. Static deformations of the tube-block structure for two tube thicknesses (a) $h = 1.0$ mm and (b) $h = 2.0$ mm at the compressive load $p = 0.75$ MPa. It is noted that the deformation is enlarged by five times.

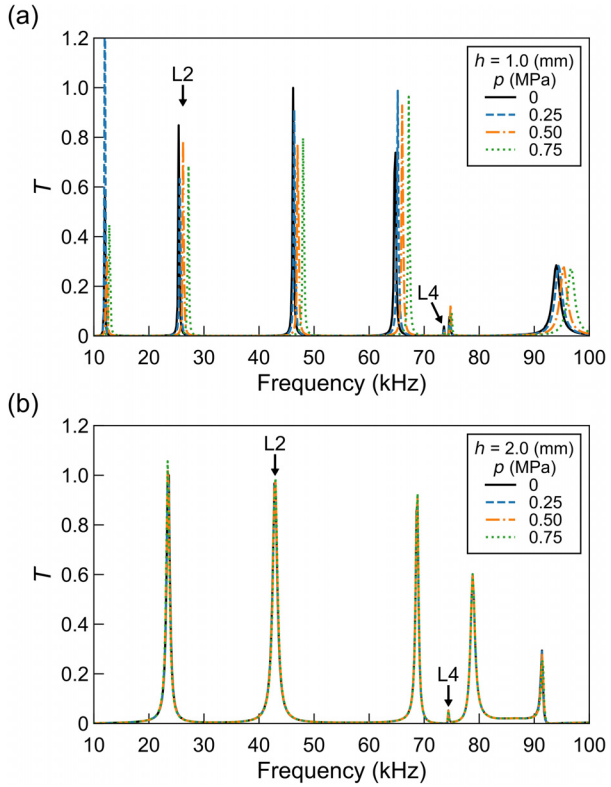

FIG. 13. (Color online) Effects of the compressive load p on the frequency dependence of the transmission ratios for the L wave incidence, calculated for two tube thicknesses (a) $h = 1.0$ mm and (b) $h = 2.0$ mm at fixed dimensions $R = 10$ mm, $W = 40$ mm, and $2a = 0.1$ mm.

and 2.0 mm, respectively. For simplicity, the normalized quantities are not used here. In Fig. 13(a), i.e., at $h = 1.0$ mm, it is found that some peaks in the transmission ratio shift rightward as the compressive load p increases. For example, a peak labeled L2 is located at 25.4 kHz on the condition of $p = 0$, moving to 27.2 kHz at $p = 0.75$ MPa. This variation corresponds to a 7.09% shift of the peak frequency. The above feature implies that the periodically aligned tubes act as a tunable meta-interface for the elastic wave transmission between two solid blocks. On the other hand, the frequency of a peak called L4 is unchanged at 73.6 kHz, even if the load p increases. When the tube is relatively thick, i.e., at $h = 2.0$ mm in Fig. 13(b), the peak frequencies of the transmission ratio are almost invariant even if the compressive load increases from $p = 0$ to 0.75 MPa.

As described in Sec. IV B, the peaks of the transmission ratios appear due to the different resonance mechanisms. This feature implies that the shift amounts of the peak frequencies by the compressive load depend on the types of the peaks. Figures 14(a) and 14(b) show the displacement distributions for the L wave incidence at the two peak frequencies of L2 and L4, respectively, indicated in Fig. 13(a). Each figure shows the displacement magnitude of the harmonic component at $p = 0$. The displacement fields at the peak frequencies L2 and L4 represent the local resonances of the tube and block surfaces, respectively. This difference corresponds to the result that the increase in the peak frequency

https://doi.org/10.1121/10.0026462

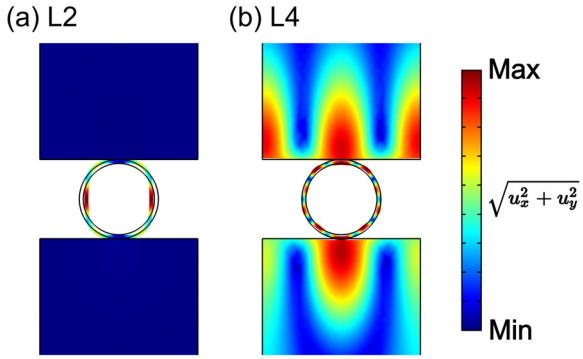

FIG. 14. (Color online) Displacement distributions at the peak frequencies of (a) L2 and (b) L4 for the L wave incidence at the tube thickness $h = 1.0$ mm and the compressive load $p = 0$. In each figure, the color represents the magnitude of the displacement vector of the harmonic component.

L2 with increasing compressive load p is more apparent than that of L4. Namely, the deformation of the tube affects its own resonance characteristics, but the Rayleigh wave resonance on the block surfaces is unchanged.

For a relatively thick tube, i.e., at $h = 2.0$ mm, the shifts of the peak frequencies in Fig. 13(b) are not as clear as those at $h = 1.0$ mm in Fig. 13(a) because of the static deformations shown in Figs. 12(a) and 12(b). At a fixed compressive load, the static deformation of the tube tends to decrease as the thickness increases because the stiffness increases. When the local structure shows large deformation by a static load, the shift of the peak frequencies corresponding to its local resonance in the transmission ratio would become significant.

In this paper, the effect of the compressive loading on the peak frequencies of the transmission ratio has been presented only for the L wave incidence. In fact, it is confirmed that analogous phenomena appear in the case of the T wave incidence, which is omitted in the present paper. In actual measurements, since the attenuation of the T wave is generally more serious than that of the L wave, the resonance behavior for the T wave incidence could be different.

In the numerical model of the present study, the tube-block structure consists of linear elastic material, e.g., aluminum alloy. In actual experiments, however, such an assumption would sometimes be inappropriate when tuning the resonance frequencies. As shown above, large deformation is necessary to apparently shift the peak frequencies in the transmission ratio, requiring large static loads in the case of metal structures. If the tube-block structure is produced with soft materials, such as rubbers, it would show sufficiently large deformation at lower loads to make the resonance frequencies tunable more easily. In that case, the model of hyperelastic materials should be used to predict the resonance characteristics similarly to Refs. 20, 23, and 24. It would be also necessary to carefully consider the effects of the damping properties of the materials on the resonance characteristics.

It is also noted that the numerical model for the static deformation analysis is simplified in this study. If the tubes undergo large deformation, instabilities, such as buckling and plastic deformation, would occur. Stress concentration at the joints between the tubes and the blocks could be another issue in predicting the wave resonance characteristics more precisely. It is necessary to consider these effects in the actual tuning of the resonance frequencies, but they are not further examined in the present study. Experimental validation for the numerical results shown in this paper remains as future work. It would be necessary to discuss the detailed parameters of the structure dimensions and the frequency ranges through the experimental validation process.

V. CONCLUSIONS

In this study, the transmission and resonance characteristics of elastic waves in a tube-block structure have been investigated by FE simulations. The proposed structure consists of periodically aligned tubes sandwiched and joined by two blocks. For the normal incidence of a plane elastic wave, the energy flux of the transmitted wave across the tube in a unit structure has been calculated in the frequency domain to obtain the transmission ratio. As a result, it has been shown that the transmission ratios take peaks at multiple frequencies both for the longitudinal and transverse wave incidence. The wavefields at some peak frequencies have been characterized by the vibrations of the tube, while those at the other peak frequencies have shown local vibrations near the block surfaces. Eigenfrequency analysis has demonstrated that the peaks in the transmission ratios are closely related to the local resonance of the tube and the Rayleigh wave resonance on the block surfaces. This fact has been consistent with the numerical results that the peak frequencies originating from the tube resonance depend on the tube dimensions, while the ones associated with the Rayleigh wave resonance vary dominantly with the tube interval. Furthermore, it has been shown that some peak frequencies increase when the structure is subjected to compressive loading. Their shift amounts have been associated with the vibration patterns at the peak frequencies. Specifically, the peak frequencies corresponding to the local resonance of the tube have shifted more significantly than those to the Rayleigh wave resonance.

AUTHOR DECLARATIONS

Conflict of Interest

The authors have no conflicts to disclose.

DATA AVAILABILITY

The data that support the findings of this study are available from the corresponding author upon reasonable request.

[1]M. Cai, O. Painter, and K. J. Vahala, "Observation of critical coupling in a fiber taper to a silica-microsphere whispering-gallery mode system," Phys. Rev. Lett. **85**(1), 74–77 (2000).
[2]A. Yariv, "Critical coupling and its control in optical waveguide-ring resonator systems," IEEE Photonics Technol. Lett. **14**(4), 483–485 (2002).

[3]I. M. White, H. Oveys, and X. Fan, "Liquid-core optical ring-resonator sensors," Opt. Lett. **31**(9), 1319–1321 (2006).
[4]Y. Sun and X. Fan, "Optical ring resonators for biochemical and chemical sensing," Anal. Bioanal. Chem. **399**(1), 205–211 (2011).
[5]W. Fu, Z. Shen, Y. Xu, C.-L. Zou, R. Cheng, X. Han, and H. X. Tang, "Phononic integrated circuitry and spin-orbit interaction of phonons," Nat. Commun. **10**(1), 2743 (2019).
[6]O. A. Kaya, N. Korozlu, D. Trak, Y. Arslan, and A. Cicek, "One-dimensional surface phononic crystal ring resonator and its application in gas sensing," Appl. Phys. Lett. **115**(4), 041902 (2019).
[7]A. Biçer, "Acoustic add-drop filter involving a ring resonator based on a one-dimensional surface phononic crystal," Ultrasonics **117**, 106551 (2021).
[8]W. M. Robertson, C. Vazquez, A. LaVerde, A. Wassenberg, C. Olson, and J. Lopez, "Acoustic ring resonator: Experiments and simulations," AIP Adv. **12**(1), 015006 (2022).
[9]A. Khelif, A. Choujaa, S. Benchabane, B. Djafari-Rouhani, and V. Laude, "Guiding and bending of acoustic waves in highly confined phononic crystal waveguides," Appl. Phys. Lett. **84**(22), 4400–4402 (2004).
[10]R. Sainidou, N. Stefanou, I. E. Psarobas, and A. Modinos, "A layer-multiple-scattering method for phononic crystals and heterostructures of such," Comput. Phys. Commun. **166**, 197–240 (2005).
[11]J. Mei, Z. Liu, and C. Qiu, "Multiple-scattering theory for out-of-plane propagation of elastic waves in two-dimensional phononic crystals," J. Phys: Condens. Matter **17**, 3735–3757 (2005).
[12]Y. Pennec, J. O. Vasseur, B. Djafari-Rouhani, L. Dobrzyński, and P. A. Deymier, "Two-dimensional phononic crystals: Examples and applications," Surf. Sci. Rep. **65**(8), 229–291 (2010).
[13]M. I. Hussein, M. J. Leamy, and M. Ruzzene, "Dynamics of phononic materials and structures: Historical origins, recent progress, and future outlook," Appl. Mech. Rev. **66**(4), 040802 (2014).
[14]O. R. Bilal and M. I. Hussein, "Trampoline metamaterial: Local resonance enhancement by springboards," Appl. Phys. Lett. **103**, 111901 (2013).
[15]P. Wei, C. Croënne, S. Tak Chu, and J. Li, "Symmetrical and anti-symmetrical coherent perfect absorption for acoustic waves," Appl. Phys. Lett. **104**(12), 121902 (2014).
[16]G. Ma and P. Sheng, "Acoustic metamaterials: From local resonances to broad horizons," Sci. Adv. **2**(2), e1501595 (2016).
[17]H. Zhong, Y. Gu, B. Bao, Q. Wang, and J. Wu, "2D underwater acoustic metamaterials incorporating a combination of particle-filled polyurethane and spiral-based local resonance mechanisms," Compos. Struct. **220**, 1–10 (2019).
[18]Q. Lin, J. Zhou, K. Wang, D. Xu, G. Wen, Q. Wang, and C. Cai, "Low-frequency locally resonant band gap of the two-dimensional quasi-zero-stiffness metamaterials," Int. J. Mech. Sci. **222**, 107230 (2022).
[19]S. Yves and A. Alù, "Extreme anisotropy and dispersion engineering in locally resonant acoustic metamaterials," J. Acoust. Soc. Am. **150**(3), 2040–2045 (2021).
[20]K. Bertoldi and M. C. Boyce, "Wave propagation and instabilities in monolithic and periodically structured elastomeric materials undergoing large deformations," Phys. Rev. B **78**(18), 184107 (2008).
[21]P. Wang, F. Casadei, S. Shan, J. C. Weaver, and K. Bertoldi, "Harnessing buckling to design tunable locally resonant acoustic metamaterials," Phys. Rev. Lett. **113**(1), 014301 (2014).
[22]S. Babaee, N. Viard, P. Wang, N. X. Fang, and K. Bertoldi, "Harnessing deformation to switch On and off the propagation of sound," Adv. Mater. **28**(8), 1631–1635 (2016).
[23]P. I. Galich, N. X. Fang, M. C. Boyce, and S. Rudykh, "Elastic wave propagation in finitely deformed layered materials," J. Mech. Phys. Solids **98**, 390–410 (2017).
[24]W. Zhou, B. Wu, Muhammad, Q. Du, G. Huang, C. Lü, and W. Chen, "Actively tunable transverse waves in soft membrane-type acoustic metamaterials," J. Appl. Phys. **123**(16), 165304 (2018).
[25]Y.-F. Wang, Y.-Z. Wang, B. Wu, W. Chen, and Y.-S. Wang, "Tunable and active phononic crystals and metamaterials," Appl. Mech. Rev. **72**(4), 040801 (2020).
[26]W. Zhou, B. Wu, Y. Su, D. Liu, W. Chen, and R. Bao, "Tunable flexural wave band gaps in a prestressed elastic beam with periodic smart resonators," Mech. Adv. Mater. Struct. **28**(3), 221–228 (2021).
[27]G. Wen, S. Zhang, H. Wang, Z.-P. Wang, J. He, Z. Chen, J. Liu, and Y. M. Xie, "Origami-based acoustic metamaterial for tunable and broadband sound attenuation," Int. J. Mech. Sci. **239**, 107872 (2023).
[28]F. Casadei, T. Delpero, A. Bergamini, P. Ermanni, and M. Ruzzene, "Piezoelectric resonator arrays for tunable acoustic waveguides and metamaterials," J. Appl. Phys. **112**(6), 064902 (2012).
[29]Y. Chen, X. Li, H. Nassar, G. Hu, and G. Huang, "A programmable metasurface for real time control of broadband elastic rays," Smart Mater. Struct. **27**(11), 115011 (2018).
[30]L. Gu, C. Zhao, K. Wang, S. Li, X. Wang, and Z. Huang, "Asymmetric sound absorption achieved by double-layer piezoelectric metamaterials with tunable shunt circuit," Appl. Phys. Lett. **119**(13), 131903 (2021).
[31]Y.-Y. Peng, Z.-Z. Yang, Z.-L. Zhang, X.-Y. Zou, C. Tao, and J.-C. Cheng, "Tunable acoustic metasurface based on tunable piezoelectric composite structure," J. Acoust. Soc. Am. **151**(2), 838–845 (2022).
[32]V. Candido de Sousa, C. Sugino, C. De Marqui Junior, and A. Erturk, "Adaptive locally resonant metamaterials leveraging shape memory alloys," J. Appl. Phys. **124**(6), 064505 (2018).
[33]X.-F. Lv, S.-F. Xu, Z.-L. Huang, and K.-C. Chuang, "A shape memory alloy-based tunable phononic crystal beam attached with concentrated masses," Phys. Lett. A. **384**(2), 126056 (2020).
[34]Y. Song and Y. Shen, "A tunable phononic crystal system for elastic ultrasonic wave control," Appl. Phys. Lett **118**(22), 224104 (2021).
[35]A. Sasaki, N. Mori, and T. Hayashi, "Numerical analysis of elastic wave resonator using deformation of tube," in *Proceedings of Symposium on Ultrasonic Electronics* (2023), Vol. 44, 1P2–13.
[36]T. Pialucha and P. Cawley, "The detection of thin embedded layers using normal incidence ultrasound," Ultrasonics **32**(6), 431–440 (1994).
[37]N. Mori and T. Hayashi, "Ultrasonic interference and critical attenuation in metal-plastic bilayer laminates," J. Sound Vib. **547**, 117531 (2023).
[38]K. F. Graff, *Wave Motion in Elastic Solids* (Dover Publications, New York, 1991).
[39]W. Ke, M. Castaings, and C. Bacon, "3D finite element simulations of an air-coupled ultrasonic NDT system," NDT&E Int. **42**(6), 524–533 (2009).
[40]D. C. Gazis, "Exact analysis of the plane-strain vibrations of thick-walled hollow cylinders," J. Acoust. Soc. Am. **30**(8), 786–794 (1958).
[41]T. Hayashi, "Energy trapping of circumferential resonant modes at a thin-walled groove in a hollow cylinder," J. Acoust. Soc. Am. **146**(4), EL376–EL380 (2019).
[42]Y. Pao and U. Gamer, "Acoustoelastic waves in orthotropic media," J. Acoust. Soc. Am. **77**(3), 806–812 (1985).
[43]N. Gandhi, J. E. Michaels, and S. J. Lee, "Acoustoelastic Lamb wave propagation in biaxially stressed plates," J. Acoust. Soc. Am. **132**(3), 1284–1293 (2012).